Autonomous Oscillations and Pattern Formation with Zero External Resistance during Silicon Electrodissolution

Maximilian Patzauer, Richard Hueck, Anton Tosolini, Konrad Schönleber, Katharina Krischer[1]

Nonequilibrium Chemical Physics, Department of Physics, Technical University of Munich, 85747 Garching, Germany

Abstract

We report the existence of small autonomous amplitude oscillations without the presence of an external series resistor during electrodissolution of both p- and highly illuminated n-type Si electrodes in a 60 mM NH_4F electrolyte at pH 1. This finding enabled us to study possible emergence of patterns without the presence of the global coupling induced by an external resistance. While with p-type electrodes we could not find a spatial bifurcation upon varying the parameters, stable domain-type patterns with distinct dynamics formed spontaneously when lowering the illumination intensity. Their emergence could be linked to the lateral coupling through valence band holes. Experiments where only part of the electrode was illuminated gave further insight into the role of the hole dynamics for the formation of spatio-temporal dissipative structures.

Keywords: silicon electrochemistry, electrochemical oscillations, reaction diffusion system, chimera states, nonlinear dynamics

1. Introduction

Oscillations during Si electrodissolution have attracted an unbroken interest since their discovery more than half a century ago [1]. They occur in wide parameter ranges and were studied with a multitude of methods, most of the studies focusing on elucidating the oscillation mechanism (for an overview see chapter 5 in [2]). Yet, the origin of the oscillations could not yet be explained satisfactorily. The main approaches are discussed in [3–8]. A more recent publication from our group points to the existence of different types of oscillations, most likely involving different feedback loops [9]. We have also started to investigate the formation of spatio-temporal patterns in the oxide layer thickness with an emphasis on elucidating the universal properties of the self-organisation phenomena [10–12].

Among the observed patterns were so-called chimera states [11, 12], a dynamical state that received an enormous attention during the last decade in the nonlinear dynamic community [13]. Chimera states form in oscillatory systems, or ensembles of identical, coupled oscillators, and denote states which are composed of parts which oscillate in synchrony and parts that exhibit incoherent oscillations with different mean frequencies. The formation of such a state is highly counter intuitive, exhibiting the opposite behaviour of what we experience in everyday life, namely the synchronisation of oscillators with different frequencies [14]. Yet, chimera states might be linked to phenomena such as unihemispheric sleep, blackouts in power grids, or bump-states observed in neural systems [13], which calls for detailed theoretical and experimental studies in laboratory settings. As for the latter, truly self-organised chimera states were first observed in the Si electrodissolution system. Here, 'truly self-organised' indicates that they formed spontaneously with neither a computer fed back spatial coupling nor special preparation of initial condition as in most other experimental realisations [15–19], and it remains one of the few experimental systems in which their emergence and properties can be studied. The Si electrodissolution chimera states were found for n-type Si electrode under moderate illumination intensities, and the spatial coupling through the illumination is believed to be responsible for their emergence. With a generic model assuming a nonlinear global coupling the observed states could be reproduced [11, 20], however, a link between the physical and electrochemical quantities and the model parameters has still to be established.

An understanding of what triggers the emergence of chimera states during Si electrodissolution requires more insight in the spatial coupling. In the experiments conducted so far in our group, there were mostly two sources of spatial coupling present, a global coupling induced by an external ohmic series resistance and coupling through valence band holes imposed by the reduced illumination intensity [12].

In this paper, we present experiments that focus on further insights into the impact of the spatial coupling through valence band holes on pattern formation. Therefore, no external resistance is used throughout. We first show that self-sustained current oscillations with a very small amplitude also exist without an external ohmic series resistance for both p-type and highly illuminated n-type electrodes. Then, we demonstrate that reducing the illumination n-type Si leads to a spatial symmetry breaking, and even to the coexistence of coherently and incoherently oscillating parts of the electrode surface, reminiscent of chimera states.

[1] Corresponding author: krischer@tum.de

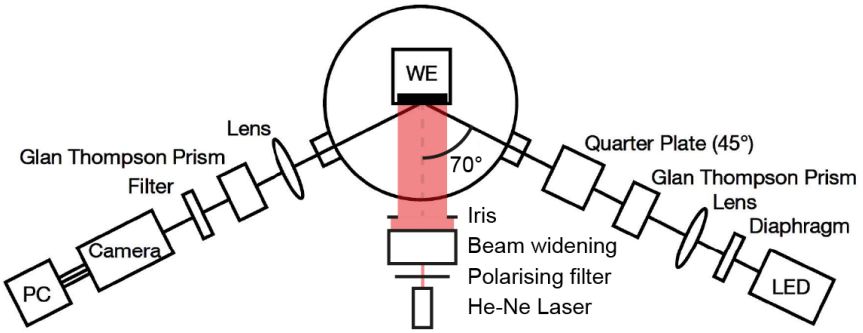

Figure 1: Illustration of the optical set-up used for the in-situ measurements of the Si electrode surface.

2. Experimental

2.1. Sample preparation

The experiments were conducted with single crystalline Si (111) wafers with a resistivity of 5-25 Ωcm (p-doped) or 1-10 Ωcm (n-doped). To ensure an ohmic back contact a 200 nm Al layer was thermally evaporated and annealed at 400 °C for 30 min (p-doped) or at 250 °C for 15 min (n-doped) under 100 mbar nitrogen atmosphere. The Si wafers were treated with an oxygen plasma at 200 W for 5 min under 1.4 mbar oxygen atmosphere, mounted on a custom made polytetrafluoroethylene (PTFE) holder, contacted with silver paste on the back, and sealed using silicone rubber (Scrintex 901, Ralicks GmbH, Rees-Haldern, Germany), leaving an opening of 15-25 mm^2. Before the experiment the mounted working electrode was cleaned from organic contamination and dust by first gently wiping it with a tissue drenched in acetone (Merck, p.a.) and subsequently immersing it in acetone (Merck, p.a.) (10 min), ethanol (Merck, p.a.) (5 min), methanol (Merck, p.a.) (5 min) and ultra pure water (18.2 MΩcm) (5 min).

2.2. Electrolyte

An aqueous solution, prepared with ultra pure water (18.2 MΩcm), containing 60 mM NH_4F (Merck, p.a.) and 142 mM H_2SO_4 (Merck, Suprapur) with a total volume of 500 ml was used as electrolyte for all experiments, if not mentioned otherwise. Literature values [21] for the dissociation constants of HF and H_2SO_4 were used to calculate the pH value to be 1.

2.3. Electrochemical Set-up

The experiment was performed in a custom-made three electrode electrochemical cell with a circular shaped platinum wire (99.99%, Chempur), $\oslash \approx 5$ cm, as counter electrode and a commercial $Hg|Hg_2SO_4$ reference electrode. The counter electrode was placed symmetrically in front of the working electrode and the reference electrode several centimetres behind the working electrode. All PTFE and platinum parts were cleaned regularly in Piranha solution. The glassware was cleaned immersing it in nitric acid and sequentially in an 1 M aqueous potassium hydroxide solution. All parts were stored in covered ultra pure water baths. Before the experiments the electrolyte was purged with argon for 30 min and constantly stirred with a magnetic stirrer at 10 Hz. The glass bubblers used for purging the electrolyte were removed before the measurements to prevent an undefined change in the fluoride concentration due to the glass dissolving in the electrolyte. An argon overpressure was kept with an additional gas inlet and the stirring was maintained throughout the experiment. The potential was controlled using a FHI-2740 potentiostat (electronic laboratory of the Fritz-Haber-Institut, Berlin, Germany) and the current and voltage were digitized using a data acquisition board (PCI-6221, National Instruments).

2.4. Ellipsometric Imaging Set-up

The ellipsometric silicon oxide detection was realised using a LED (Linos, HiLED, λ =470 nm). The light was polarised using a Glan-Thompson prism and a zero order $\lambda/4$-plate (λ = 488 nm) and then shone at the sample with an incident angle close to the Brewster angle (α = 70°) to assure maximal contrast. Upon reflection the polarisation changes depending on the optical path through the oxide. The reflected polarised light then passes through a second Glan-Thompson prism for contrast enhancement and then imaged on a charge-coupled device with 640x480 pixels (JAI CV-A50). The signal was in turn digitized using a frame grabber card (PCI-1405, National Instruments). The optical components were mounted and aligned using a microbench system (LINOS). A schematic of the optical set-up can be seen in Fig. 1.

2.5. Illumination Set-up

The illumination of the n-doped samples was realised using a linearly polarised He-Ne laser (HNL150L-EC, Thorlabs). The illumination intensity was adjusted using an adjustable polarisation filter. To assure a spatially homogeneous illumination the beam was optically expanded to a diameter of 1.5 cm and subsequently passed through an iris diaphragm so that only the central part of the beam was incident on the sample. To test for the homogeneity of the illumination, experiments were repeated using an extra mirror in the optical path of the He-Ne laser, resulting in a mirroring of possible spatial asymmetries in the illumination intensity.

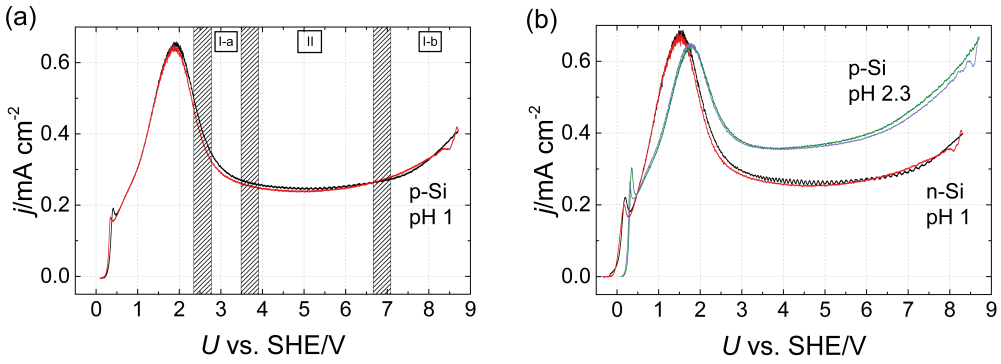

Figure 2: (a) Cyclic voltammogram (2 mV/s) of a p-Si electrode in a 60 mM aqueous NH_4F electrolyte, pH 1 (black curve - forward scan, red (grey) curve - backward scan). Region II and I-a,I-b indicate the voltage regimes where sustained and damped oscillations were found, respectively. Hashed regions indicating the approx. borders between the different regions. (b) Cyclic voltammogram (2 mV/s) of an illuminated n-Si electrode (3.88 mW/cm^2) in the electrolyte of plate (a) (black curve - forward scan, red (grey) curve - backward scan) and of a p-Si electrode (2 mV/s) in 50 mM NH_4F electrolyte (pH 2.3) (green (dark grey) curve - forward scan, blue (light grey) curve - backward scan).

3. Results

3.1. Sustained current oscillations

Figure 2a shows a cyclic voltammogram (CV) of p-doped Si in our fluoride containing base electrolyte (pH 1) taken at 2 mV/s. At this slow scan rate the current-voltage curve is quasi-stationary. The electropolishing region of Si is found at voltages below the pronounced current maximum at 2 V vs. SHE. Above this peak an oxide layer forms at the Si|electrolyte interface which is first wet and gradually turns into a rather compact, dry form that is fully developed above approximately 3 V vs. SHE [2]. When the dry oxide has formed, the oxidation current is limited by the etching rate of the oxide layer, becoming practically independent of the potential up to about 7 V vs. SHE where morphological changes in the oxide layer allow for a modest increase in oxidation current with potential. These features are well known to exist in a wide pH and fluoride concentration range [2]. In Fig. 2b, CVs obtained with a highly illuminated n-type electrode in this base electrolyte as well as with a p-type electrode in a 50 mM NH_4F electrolyte (pH2.3) are shown for comparison. Besides a shift of the n-doped CV by +350 mV, corresponding to the difference in open circuit potential, the two CVs obtained in the same electrolyte are nearly identical, especially at voltages > 2.5 V which are of interest in the context of the paper. We attribute the slight difference in the absolute values of the current density to an uncertainty of the electrode area of up to 0.5 mm^2. In contrast, the CV obtained at higher pH exhibits a higher current density in the current plateau of the dry oxide region.

A careful look at the plateau region of the CVs in our base electrolyte (pH1) reveals that in a wide potential window the plateau current is superimposed by small oscillations. Potential step experiments from the open circuit potential to a potential value within the dry oxide region were carried out to test for the stability of the oscillations. Three such experiments are depicted in Fig. 3 for potential steps to 3.15, 4.65 and 7.65 V vs. SHE. The respective two upper graphs show the current density (left) and the spatially average ellipsometric intensity (right) time series after the jump. The left graph below depicts a 2D ellipsometric snapshot of the electrode, and the right one a one-dimensional cross section through the ellipsometric images versus time. In the region of dry oxide, the ellipsometric intensity is proportional to the oxide layer thickness [22]. Clearly, in Figs. 3a and c the oscillations are damped, while in b small amplitude oscillations persist over several thousand seconds and acquire a stable amplitude. We therefore conclude that in this electrolyte the system exhibits stable oscillations without the insertion of an external resistor. In this region of sustained oscillations phase waves usually emerge on the electrode, as can be seen in the ellipsometric image of Fig. 3b. As a consequence, the local oscillation amplitude of the oxide layer was larger than the average one. In Fig. 2a the potential regions in which transient and self-sustained oscillations were found are indicated by I and II, respectively, with the borders between them shown as a hashed region, their width indicating the uncertainty in the determination of the threshold voltage which is due to the ever slower damping as the transition to sustained oscillations is reached. The low voltage border where damped oscillations start to exist could also only be determined with a relatively large uncertainty as indicated by the width of the hashed line.

In Fig. 4 the same type of measurement as in Fig. 3b is presented, but with the electrolyte used for the p-type electrode in Fig. 2b. Here, no stable autonomous oscillations were observed without an external series resistor (neither with n- nor with p-doped Si electrodes) confirming findings in the literature [4]. Note the finer colour scale compared to Fig. 3. Clearly, both the spatially averaged signal and the spatially extended signal show a continuous damping, in contrast to the behaviour in Fig. 3b, and thus in this measurement, as well as in all other measurements in this electrolyte, the system eventually reached a stationary state. In other words, no stable oscillations are found and region I-a reaches all the way to region I-b.

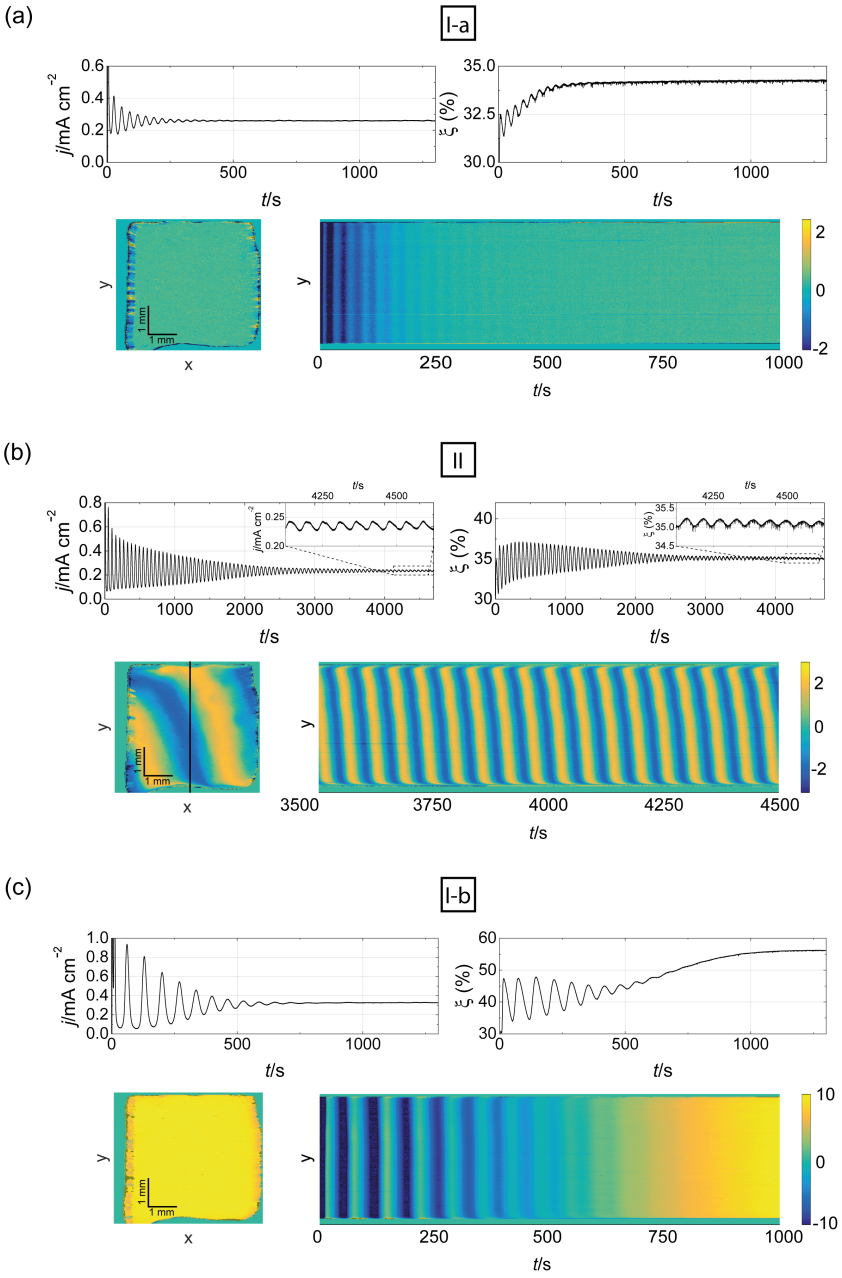

Figure 3: Dynamics found in the different regions marked in Fig. 2. Current density, j, and spatially averaged ellipsometric intensity, ξ, (top) together with the ellipsometric intensity distribution on the electrode and the temporal evolution of a 1D cut indicated in the snapshot. (a) Damped oscillations at U_{app} = 3.15 V vs. SHE, region I-a, snapshot at t = 1000 s. (b) Stable oscillations at U_{app} = 4.65 V vs. SHE, region II, snapshot at t = 4000 s. (c) Damped oscillations at U_{app} = 7.65 V vs. SHE, region I-b snapshot at t = 1000 s. All measurements with highly illuminated n-Si (3.88 mW/cm^2) in a 60 mM NH_4F solution (pH 1).

3.2. Spatial pattern formation

We demonstrated that the sustained oscillations obtained in our base electrolyte without an external series resistance were qualitatively indistinguishable for p-type and highly illuminated n-type Si electrodes. Therefore, we are now in a situation in which we can study the influence of the spatial coupling induced when lowering the illumination without the simultaneous presence of a global coupling brought about by an ohmic series resistance, as in previous published measurements on pattern formation during Si electrodissolution [10–12, 20].

Figure 5 manifests how the dynamic changes compared to the one shown in Fig. 3b when reducing the illumination intensity: The global time series of current and spatially averaged ellipsometric intensity become irregular (Fig. 5a) and the wavy arms on the electrode are deformed and exhibit strong intensity modulations (Fig. 5c). Local time series of the ellipsometric signal at positions indicated in the right snapshot of Fig. 5c are shown in Fig. 5b. The time series in the top-most plate has a clear period-2 signature (only every second maximum has the same height) and a somewhat higher base frequency (24 mHz) than the simple periodic oscillations in the lower plate. The time series shown in the middle plate exhibits irregular oscilla-

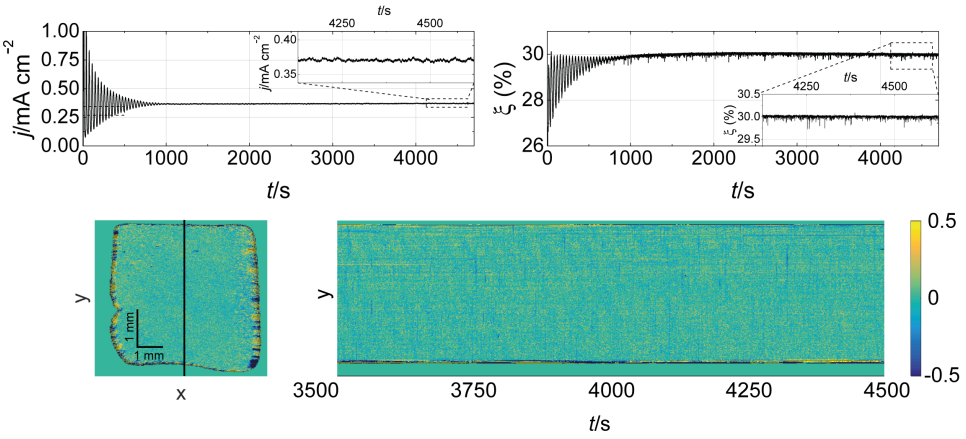

Figure 4: Current density, j, and spatially averaged ellipsometric intensity, ξ, (top) together with the spatially averaged ellipsometric intensity distribution on the electrode at t = 4000 s and the temporal evolution of a 1D cut indicated in the snapshot. U_{app} = 4.65 V vs. SHE, highly illuminated n-Si (3.88 mW/cm^2) in a 50 mM NH_4F solution (pH 2.3).

tions. Looking at the 1D cross section vs. time displayed in Fig. 5e, it becomes evident that all oscillators within this cut belong to one of these three behaviours. The fast period-2 oscillations are found in the right oscillating strip, the slower oscillations of period-1 on the left while the irregular oscillations occur in between these two regions. To identify these regions on the entire electrode, the spatial distribution of the normalised absolute value of the Fourier coefficients corresponding to the main frequencies of the period-1 sinusoidal oscillations and the period-2 oscillations are plotted in Fig. 5d. Here it can be seen that the period doubling occurs in the upper left corner of the electrode (high pink amplitude) while the lower frequency oscillations dominate in the complementary region (high red amplitude region). Note that the frequencies in the two periodically oscillating parts of the electrode are not locked and that the irregularly oscillating region mediates the dynamics between them. These patterns were found to be stable over several hours.

While reducing the illumination intensity always induced the spontaneous formation of regions with different oscillatory dynamics, the specific characteristics of the emerging pattern sensitively depended on the value of the illumination intensity. An example with a lower degree of spatial and temporal coherence is shown in Fig. 6. Here, the temporal evolution of the 1D profile suggests that there is an almost periodically oscillating region with a somewhat higher mean amplitude, flanked by incoherently oscillating regions. In general once the uniform oscillations became unstable, the coherence of the patterns tended to increase with decreasing illumination intensity. This suggest that a lower illumination intensity corresponds to a stronger coupling.

When the illumination was reduced further, both oscillations and patterns vanished, the system attaining a uniform steady state with a current density higher than the plateau current. Fig. 7 depicts how the current density and the spatially averaged ellipsometric signal developed immediately after lowering the illumination intensity during the measurement from a high value, where the system oscillated (cf. Fig. 3b), to an illumination at which the dry oxide layer was no longer stable. In the temporal evolution of the 1D cut as well as in the snapshots we see that the initially approximately uniform oxide layer quickly develops two regions with different mean thickness, one of them again being incoherent in space and time, before a uniform state with low oxide layer thickness and high current density spreads over the entire surface. The transient dynamics seem to traverse through the dynamic states that are stable in an interval of a somewhat higher illumination intensity.

So far, we have demonstrated that a lower but uniform illumination intensity induces the formation of spatial patterns or domains with different oscillation frequencies, whereby one of them might oscillate incoherently in space and time, being reminiscent of a chimera state.

A different way to probe the influence of the illumination intensity is to only illuminate a part of the electrode. In this way, a gradient in the density of valence band holes is created at the boundary of the illuminated region, such that we can expect an outward flow of holes, which mimics a gradient in the illumination intensity, and thus again sheds light on the role of the spatial coupling through charge carriers in the semiconductor and its interaction with the oxide formation/dissolution dynamics. Fig. 8 shows one such example measurement. Here, the opening of the circular aperture in the illumination path was narrowed so that only the part of the electrode inside the area indicated by the dashed circle was illuminated. The illumination intensity was set to a level below the high illumination level of Fig. 3 and above the level necessary for creating multiple domains. Under these conditions, concentric waves of slightly thicker oxide propagated from the rim of the illuminated circular region towards its center. In the course of time, the border from which these waves emerged withdrew slowly towards the center, Fig. 8 depicting a situation after about half an hour, the outer illuminated ring now taking on a constant oxide thickness. Here, the temporal average of each pixel is subtracted such that all non-oscillating parts of the electrode are set to 0. We note that after about 8 hours the illuminated surface became uniform

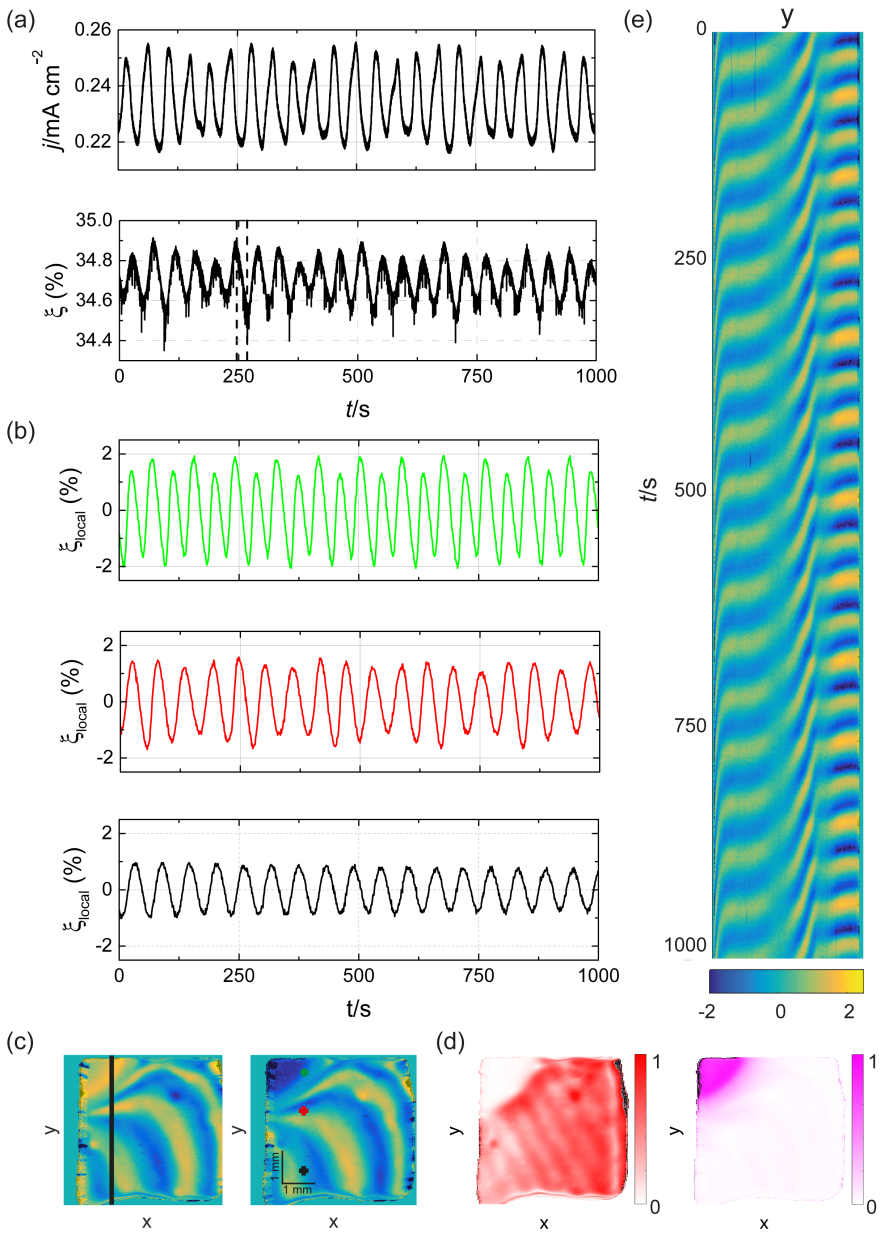

Figure 5: Two regions with different frequencies, emerging at low illumination (0.28mW/cm^2) in pH 1, [NH_4F] = 60 mM electrolyte at an applied voltage of U_{app} = 4.65 V vs. SHE. (a) Time series of the current density (top) and spatially averaged ellipsometric intensity signal (bottom). (b) Local time series of the ellipsometric intensity signal as indicated in the right snapshot in (c) in corresponding order top to bottom. (c) The ellipsometric intensity distribution on the electrode at t = 246 s (left) and t = 268 s (right) indicated by the vertical lines in (a). (d) Spatial distribution of the normalised absolute value of the Fourier coefficients corresponding to the frequency 19 mHz (red) and 24 mHz (pink). (e) Temporal evolution of a 1D cut along the line indicated in the left snapshot in (c).

and the dynamics stationary, however, due to the enormous duration of the experiment in which one can expect also minor changes in electrolyte composition and possibly also other parameters (e.g. temperature) it does not seem to be sensible to further interpret this result.

4. Discussion

Our experiments present evidence that the anodic oxidation of Si in fluoride containing electrolytes may exhibit autonomous oscillations at high anodic voltages, even when there is no external resistance present. This allowed us to investigate spatial self-organisation on the electrode surface in the oscillatory region without the presence of a linear global coupling. The latter is known to act synchronising for sinusoidal oscillations close to a Hopf bifurcation but might lead to cluster formation if the global coupling function contains higher harmonics [23]. The ellipsometric snapshot in Fig. 3b shows that in contrast to findings in the presence of an external resistance [22], the oscillations were accompanied by wave like structures, apparently propagating across the electrode. This is true for p-type as well as highly illuminated n-type Si. In successive ex-

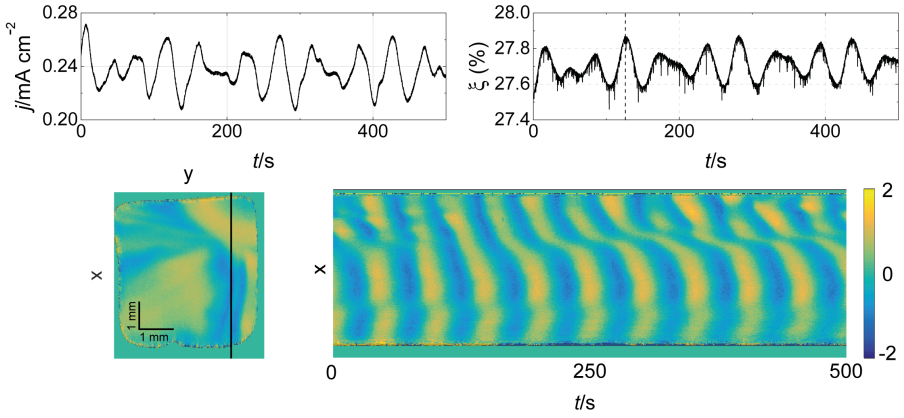

Figure 6: Current density, j, and spatially averaged ellipsometric intensity, ξ, (top) together with the ellipsometric intensity distribution on the electrode at t = 1426 s (indicated by dashed line in in the top right panel) and the temporal evolution of a 1D cut indicated in the snapshot. U_{app} = 4.65 V vs. SHE, illumination intensity 0.34 mW/cm^2, 60 mM NH_4F, pH 1.

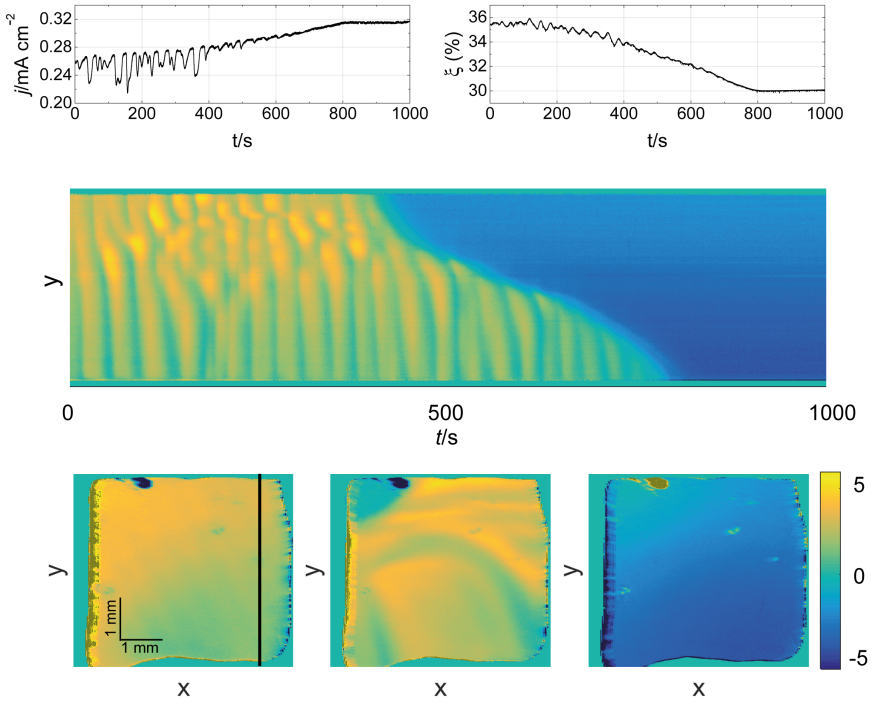

Figure 7: Current density and spatially averaged ellipsometric intensity (top), the 1D temporal evolution of the ellipsometric intensity signal at the cut indicated in the snapshot (middle) together with the ellipsometric intensity distribution on the electrode (t = 0 s, t = 185 s, t = 900 s) (bottom). U_{app} = 4.65 V vs. SHE, 0.25 mW/cm^2) in a 60 mM NH_4F solution (pH 1).

periments with different samples the orientation of the waves was always the same. Furthermore, the wavelength decreased over time. We attribute these waves to a slight parameter gradient in the system that in turn induces a slight gradient in the frequency distribution which implies that the apparent waves are phase waves. However, we were not able to identify the origin of the inhomogeneity. They existed in stagnant as well as in stirred electrolytes and did not seem to be related to the position of the circular-shaped counter electrode. Furthermore, the phase waves persisted when using a Cu sheet that was brought in electrical contact with the Al back contact by a Ag conductive paste over the entire area of the electrode. Therefore, we consider it unlikely that the gradient is caused by the back contact. In addition, when rotating the electrode by 180°, the phase waves kept their apparent propagation direction in laboratory frame. Therefore, we also exclude an inhomogeneity in the doping level. The most likely possibility appears to be an influence of the insulation border from the silicone seal. Regardless, our interpretation of the waves as phase waves suggests that under perfectly uniform parameter settings the oscillations would be uniform as well.

This changes when lowering the illumination intensity. At a

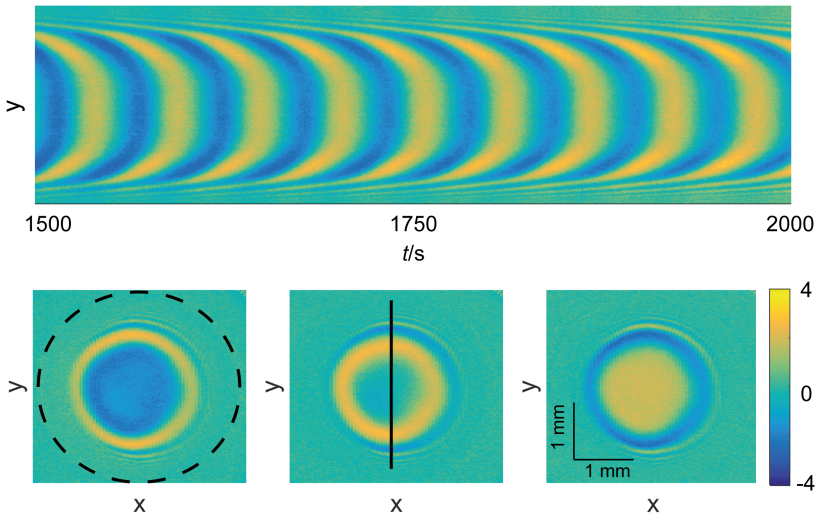

Figure 8: Resulting 1D temporal evolution of the ellipsometric intensity when only the center part of the electrode was illuminated, together with the ellipsometric intensity distribution on the electrode (t = 1730 s, t = 1745 s, t = 1760 s). The illuminated part is indicated by the dashed circle in the left most snapshot and the 1D cut is indicated in the middle most snapshot. The temporal average of each pixel was subtracted. U_{app} = 4.65 V vs. SHE, 0.78 mW/cm^2, 60 mM NH_4F solution (pH 1).

threshold intensity the electrode splits into domains with distinct temporal behaviour pointing to a spatio-temporal bifurcation induced by a destabilizing action of the spatial coupling. Since the illumination determines the number of electron-hole pairs generated, and at least the first step of the oxidation of Si involves a valence band hole, it appears obvious that a change in the illumination intensity affects the spatial coupling through diffusion (or migration) of holes. As long as the oxidation current is limited by the etch rate or, equivalently, by migration of ions through the oxide, the dynamics is insensitive upon fluctuations of the concentration of holes at the Si|SiO_2 interface. However, when the internal photon flux (i.e. the flux corrected for reflection losses) comes close to the faradaic charge carrier flux, i.e. when the momentary internal quantum efficiency Φ approaches 1, Si atoms in the Si|SiO_2 interfacial region start to compete for holes, any lateral hole concentration difference being translated in both different local hole capture rates and a lateral hole flux.

This picture is supported by the experiments in which only a circular region of the electrode was illuminated, cf. Fig. 8. As long as the illumination intensity was high enough to allow for an internal quantum efficiency (related to the mean current density) considerably below 1, phase waves developed within the illuminated circle identical to the ones found when the entire electrode was illuminated. Only when Φ approached 1 did the outward flow of holes affect the dynamics inside the illuminated region and concentric waves emerged from the illuminated rim propagating towards the center. Fig. 8 depicts an example with $\Phi \approx 0.9$, where the phase waves were replaced by such a border induced target wave pattern.

The formation of patterns on an entirely illuminated electrode only took place at considerably lower illumination intensities, i.e. Φ considerably larger than 1. For example, in the experiments shown in Figs. 5 and 6, Φ was approximately 2.3 and 2, respectively. Therefore, charge carriers not created through the absorption of a photon must be involved in the oxidation process. Under our experimental conditions, it seems to be most likely that these are valence band holes that are created through tunnelling of valence band electrons into the conduction band. Note that a quantum efficiency larger than 1 during Si electrodissolution in NH_4F electrolyte was reported before at low voltages where the Si surface is not covered by an oxide [24]. Here, the photocurrent multiplication could be explained by the injection of electrons into the conduction band of the dissolving Si atoms. A value of $\Phi \approx 2$ thus signifies that at least two charge carriers that are not generated through photon absorption are involved in the four-electron oxidation of a Si atom. Despite this change in hole generation mechanism, the overall rate of oxidation is still the same as at high illumination intensity and the oxide layer (as measured through the ellipsometric intensity) is hardly effected in thickness or quality. These considerations are in agreement with the assumption that the spatial instability is induced by lateral coupling between different parts of the electrode through diffusion and migration of holes (hole-transport induced spatial instability).

At even lower illumination intensities, oscillations and patterns occurred only transiently (cf. Fig. 7), the system attaining a steady state with higher current density and thinner oxide layer thickness. Here, with respect to the initial mean current density, which is close to the dry oxide plateau current density, Φ was about 2.8. This value increased to 3.6 at the attained current density. A steady state current density well above the value of the plateau current at high illumination intensity implies a faster etch rate of the oxide, which in turn reflects a change in oxide composition or morphology under low illumination conditions. In addition, it changes the photodissolution of Si from etch rate limited to kinetically limited, inducing a feedback loop: A decrease in the hole concentration (due to the

lower illumination intensity) slows down the oxide formation rate, disturbing the balance between oxide formation and dissolution in favour of a faster dissolution. This, in turn, results in a thinner oxide layer that obviously promotes the generation rate of charge carriers in the dark, and therewith a higher current density.

5. Conclusion

In this paper, we demonstrated that the electrodissolution of p- and n-type Si may exhibit autonomous oscillations which are stable over several hours without an external series resistance. Exploiting the illumination intensity as a bifurcation parameter, we study the impact of the illumination intensity on the dynamic behaviour of n-type Si electrodes. In this way we could eliminate the presence of a global coupling mediated through the external control that had been present in all previously published pattern formation experiments. At high illumination intensities the system tended to form phase waves but does not possess a true spatial bifurcation. However, the latter could be induced when the photon flux was lowered to an intermediate level. In contrast to previously published patterns found in the Si electrodissolution system, the ones presented here are found at different parameters and do not involve illumination limited current plateaus. Yet, the electrode splits into different domains with distinct dynamics, similarly to the patterns reported in the literature. These patterns include states reminiscent of chimera patterns, their mechanism of formation being one of the crucial questions in nonlinear dynamics. We demonstrated that the spatial coupling through valence band holes seems sufficient to cause the emergence of coexistence patterns, which is a first step towards the elucidation of the properties of the spatial coupling.

Acknowledgments

We thank Qi Li and Munir Salman for experimental support and fruitful discussions and one referee for helpful remarks concerning the photocurrent multiplication in our experiments. Financial support from the Institute for Advanced Study - Technische Universität München, funded by the German Excellence Initiative, and the cluster of excellence Nanosystems Initiative Munich (NIM) is gratefully acknowledged.

References

[1] D. R. Turner, Electropolishing silicon in hydrofluoric acid solutions, J. Electrochem. Soc. 105 (1958) 402–408.

[2] X. G. Zhang, Electrochemistry of silicon and its oxides, Kluwer Academic, 2001.

[3] J. N. Chazalviel, Ionic processes through the interfacial oxide in the anodic dissolution of silicon, Electrochim. Acta 37 (1992) 865.

[4] J. N. Chazalviel, F. Ozanam, M. Etman, F. Paolucci, L. M. Peter, J. Stumper, The p-Si/fluoride interface in the anodic region: Damped and/or sustained oscillations, J. Electroanal. Chem. 327 (1-2) (1992) 343–349.

[5] H. J. Lewerenz, Spatial and temporal oscillation at Si(111) electrodes in aqueous fluoride-containing solution, J.Phys. Chem. B 101 (14) (1997) 2421–2425.

[6] E. Foca, J. Carstensen, H. Föll, Modelling electrochemical current and potential oscillations at the Si electrode, J. Electroanal. Chem. 603 (2) (2007) 175–202.

[7] H. Föll, M. Leisner, A. Cojocaru, J. Carstensen, Self-organization phenomena at semiconductor electrodes, Electochim. Acta 55 (2009) 327 – 339.

[8] J. Proost, F. Blaffart, S. Turner, H. Idrissi, On the origin of damped electrochemical oscillations at silicon anodes (revisited), Chem. Phys. Chem. 15 (2014) 3116.

[9] K. Schönleber, K. Krischer, High-amplitude versus low-amplitude current oscillations during the anodic oxidation of p-type silicon in fluoride containing electrolytes, Chem. Phys. Chem. 13 (2012) 2989.

[10] I. Miethe, V. Garcia-Morales, K. Krischer, Irregular subharmonic cluster patterns in an autonomous photoelectrochemical oscillator, Phys. Rev. Lett. 102 (2009) 194101.

[11] L. Schmidt, K. Schönleber, K. Krischer, V. Garcia-Morales, Coexistence of synchrony and incoherence in oscillatory media under nonlinear global coupling, Chaos 24(1) (2014) 013102.

[12] K. Schönleber, C. Zensen, A. Heinrich, K. Krischer, Pattern formation during the oscillatory photoelectrodissolution of n-type silicon: turbulence, clusters and chimeras, New J. Phys. 16 (2014) 063024.

[13] M. J. Panaggio, D. M. Abrams, Chimera states: coexistence of coherence and incoherence in networks of coupled oscillators, Nonlinearity 28 (2015) R67.

[14] A. Pikovsky, M. Rosenblum, J. Kurths, Synchronization - A Universal Concept in Nonlinear Sciences, Cambridge University Press), 2001.

[15] A. M. Hagerstrom, T. E. Murphy, R. Roy, P. Hövel, I. Omelchenko, E. Schöll, Experimental observation of chimeras in coupled-map lattices, Nature Phys. 8 (2012) 658.

[16] M. R. Tinsley, N. Simbarashe, K. Showalter, Chimera and phase-cluster states in populations of coupled chemical oscillators, Nature Phys. 8 (2012) 662.

[17] E. A. Martens, S. Thutupalli, A. Fourrire, O. Hallatschek, Chimera states in mechanical oscillator networks, Proc. Natl. Acad. Sci. 110(26) (2013) 10563.

[18] S. Nkomo, M. R. Tinsley, K. Showalter, Chimera states in populations of nonlocally coupled chemical oscillators, Physical Review Letters 110 (24) (2013) 244102.

[19] M. Wickramasinghe, I. Z. Kiss, Spatially organized dynamical states in chemical oscillator networks: Synchronization, dynamical differentiation, and chimera patterns, PLoS One 8 (2013) e80586.

[20] L. Schmidt, K. Schönleber, V. Garcia-Morales, K. Krischer, Engineerign of chemical complexity 2 (World Scientific lecture notes in complex systems - Vol. 12), World Scientific, 2014, Ch. 14, p. 239.

[21] S. Cattarin, I. Frateur, M. Musiani, B. Tribouillet, Electrodissolution of p-Si in acidic fluoride media, J. Electrochem. Soc. 147 (2000) 3277.

[22] I. Miethe, K. Krischer, Ellipsomicroscopic studies of the anodic oxidation of p-type silicon in fluoride containing electrolytes during current oscillations, J. Electroanal. Chem. 666 (2012) 1.

[23] K. Okuda, Variety and generality of clustering in globally coupled oscillators, Physica D 63 (1993) 424.

[24] H. J. Lewerenz, J. Stumper, L. M. Peter, Deconvolution of charge injection steps in quantum yield multiplication on silicon, Phys. Rev. Lett. 61 (17) (1988) 1989.